Phase locking and multiple oscillating attractors for the coupled mammalian clock and cell cycle

Céline Feillet[a,1], Peter Krusche[b,1], Filippo Tamanini[c,1], Roel C. Janssens[c], Mike J. Downey[b], Patrick Martin[a], Michèle Teboul[a], Shoko Saito[c,2], Francis A. Lévi[b,d], Till Bretschneider[b], Gijsbertus T. J. van der Horst[c,3], Franck Delaunay[a,3], and David A. Rand[b,3]

[a]Université Nice Sophia Antipolis, Centre National de la Recherche Scientifique, Institut National de la Santé et de la Recherche Médicale, Institut de Biologie Valrose, 06108 Nice, France; [b]Systems Biology Centre, University of Warwick, Coventry CV4 7AL, United Kingdom; [c]Department of Genetics, Erasmus University Medical Center, 3015 CE, Rotterdam, The Netherlands; and [d]Institut National de la Santé et de la Recherche Médicale, Unité Mixte de Recherche S776 "Rythmes biologiques et cancers," Paul Brousse Hospital, 94804 Villejuif, France

Edited by Eric D. Siggia, The Rockefeller University, New York, NY, and approved May 23, 2014 (received for review November 10, 2013)

Daily synchronous rhythms of cell division at the tissue or organism level are observed in many species and suggest that the circadian clock and cell cycle oscillators are coupled. For mammals, despite known mechanistic interactions, the effect of such coupling on clock and cell cycle progression, and hence its biological relevance, is not understood. In particular, we do not know how the temporal organization of cell division at the single-cell level produces this daily rhythm at the tissue level. Here we use multispectral imaging of single live cells, computational methods, and mathematical modeling to address this question in proliferating mouse fibroblasts. We show that in unsynchronized cells the cell cycle and circadian clock robustly phase lock each other in a 1:1 fashion so that in an expanding cell population the two oscillators oscillate in a synchronized way with a common frequency. Dexamethasone-induced synchronization reveals additional clock states. As well as the low-period phase-locked state there are distinct coexisting states with a significantly higher period clock. Cells transition to these states after dexamethasone synchronization. The temporal coordination of cell division by phase locking to the clock at a single-cell level has significant implications because disordered circadian function is increasingly being linked to the pathogenesis of many diseases, including cancer.

coupled oscillators | oscillations | circadian rhythms | gating

Most organisms adapt their physiology and behavior to daily environmental cycles by means of endogenous circadian clocks. In mammals, the circadian timekeeping system involves a master pacemaker in the suprachiasmatic nuclei that coordinates peripheral oscillators in each cell of most organs and tissues. The core mechanism governing all these clocks is a self-sustained time-delayed transcriptional/posttranslational negative feedback loop relying on clock genes (1). This genetic oscillator conveys circadian rhythmicity to physiological outputs through the regulation of a substantial and tissue-specific set of target genes or proteins.

Several critical cell cycle components have recently been found to be clock-controlled. For instance, in mice the circadian clock regulates the cyclin-dependent kinase inhibitors *p16* and *p21*, the G2/M kinase *Wee1*, as well as the checkpoint proteins CHK1 and 2, and genetic disruption of any of these links compromises cellular proliferation (2–5). Although these molecular links provide a partial mechanistic basis for the coupling between these oscillators, the consequences for the joint dynamics are far from clear, as is the extent to which the cell cycle is coordinated by the clock, and vice versa.

One-to-one phase locking of oscillators is a well-known phenomenon where two coupled oscillators have a fixed relative phase and thus oscillate with a common frequency (6). A necessary condition for two oscillators to lock in this way is for their natural frequencies, when uncoupled, to be close and for them to be coupled strongly enough. Therefore, it is reasonable to expect that functional links as above should lead to 1:1 phase locking of the clock and cell cycle when their uncoupled periods are similar. In lower organisms, evidence of circadian coupling has been published for cyanobacteria (7, 8). Likewise, phase locking of the cell cycle of budding yeast using periodic forcing of the G1 cyclin CLN2 has been demonstrated (9). Moreover, 1:1 phase locking has been shown for mechanistically detailed mathematical and automaton models of the mammalian systems (8, 10, 11).

The evidence of circadian rhythms of cell division at the tissue or organism level (12, 13) in mammals is compatible with such 1:1 phase locking at the single-cell level but is also compatible with a model where cells may or may not divide during a circadian cycle but their division is restricted by gating. Introduced in ref. 14, gating is defined there as a control whereby there are certain clock phases in which cell division is allowed to occur and other phases in which it is forbidden, thus introducing new clock-determined checkpoints. The phase-locking and gating models are distinct because for the former, unlike the latter, in ideal noise-free systems (and approximately in stochastic systems), the two oscillators cycle in step and are synchronized over the whole cycle so that knowing the phase of one system largely determines the phase of the other.

Significance

In tissues such as bone marrow, intestinal mucosa, or regenerating liver, the daily rhythm of cell division is controlled by the cell's circadian clock. Determining how this clock organizes important processes such as cell division, apoptosis, and DNA damage repair is key to understanding the links between circadian dysfunction and malignant cell proliferation. We show that in proliferating mouse fibroblasts there is more than one way in which the clock and cell cycle synchronize their oscillations and that one of them is the biological equivalent of the phase locking first discovered by Huygens in the 17th century when he coupled two clocks together. When phase-locked two coupled oscillators have a fixed relative phase and oscillate with a common frequency.

Author contributions: G.T.J.v.d.H., F.D., and D.A.R. designed research; C.F., P.K., and F.T. performed research; R.C.J., P.M., M.T., and S.S. assisted with research; M.J.D. and T.B. designed tools for cell and lineage tracking; F.A.L. assisted with design of research; C.F., P.K., F.T., and D.A.R. analyzed data; and C.F., P.K., F.D., and D.A.R. wrote the paper.

The authors declare no conflict of interest.

This article is a PNAS Direct Submission.

[1]C.F., P.K., and F.T. contributed equally to this work.

[2]Present address: Department of Infection Biology, Faculty of Medicine, University of Tsukuba, Tsukuba, Ibaraki 305-0006, Japan.

[3]To whom correspondence may be addressed. E-mail: g.vanderhorst@erasmusmc.nl, delaunay@unice.fr, or d.a.rand@warwick.ac.uk.

This article contains supporting information online at www.pnas.org/lookup/suppl/doi:10.1073/pnas.1320474111/-/DCSupplemental.

Phase locking of the mammalian systems has never been reported. Indeed, two recent studies reported a lack of clock regulation of the mammalian cell cycle (15, 16). However, earlier work of Nagoshi et al. (17) suggested a dynamical link distinct from 1:1 phase locking. They demonstrated a three-peak distribution of cell division events when timed by the phase of the circadian clock. We show that the cells we study do 1:1 phase-lock provided they are left unsynchronized. Moreover, by perturbing the system with a synchronizing protocol we show that the coupled system has coexisting dynamically distinct oscillating regimes with a significantly longer clock period and these include behavior similar to that seen in Nagoshi et al. (17). A simple model of the coupled system illuminates our experimental results and enables us to integrate a puzzling set of dynamical phenomena. Finally, we discuss evidence suggesting that the regulation between the clock and cell cycle is bidirectional.

Results

We study NIH 3T3 mouse fibroblast cells cultured in regular medium (DMEM) supplemented with various concentrations of FBS to modulate cell-cycle length. Combining computational methods with single-live-cell imaging of the Rev-Erbα::Venus clock gene reporter and a fluorescent cell cycle reporter based on the fluorescence ubiquitination cell cycle indicator (FUCCI) (Movie S1) enables us to reconstruct the joint phase trajectory of the clock and cell cycle in single-cell lineages. We extract the phase of the clock and also the cell kinetics through the G1 and S/G2/M cell cycle phases (Fig. 1). Therefore, for each cell at each point in time t we measure the clock phase $\varphi_{cl}(t)$ and the cell cycle phase $\varphi_{cc}(t)$, both of which we take to be between 0 and 2π (Fig. 1 *C* and *D*).

Unsynchronized Cells Are 1:1 Phase-Locked. In the first study, neither the clock nor the cell cycle was experimentally synchronized to observe both oscillators as undisturbed as possible. The initial density of cells was chosen so that cells did not become confluent over the course of the experiment. The distributions of the period of the clock and the cell cycle from cells maintained in 10% FBS show mean values of 21.9 ± 1.1 h and 21.3 ± 1.3 h, respectively (Fig. 2*A* and *SI Appendix*, Fig. S2*A*). Increasing FBS to 15% significantly decreases both mean periods to 19.4 ± 0.5 h and 18.6 ± 0.6 h, respectively (Fig. 2*A* and *SI Appendix*, Fig. S2*A*).

The combined phase $\Phi(t) = (\varphi_1(t), \varphi_2(t))$ of two oscillators determines a point in the square $0 \le \varphi_1, \varphi_2 \le 2\pi$. This square should be regarded as a torus because phases are periodic and therefore opposite sides of the square should be identified (Fig. 2 *C* and *D*). Then, as time t increases the combined phase $\Phi(t)$ traces out a continuous curve on the torus. In noise-free coupled oscillators described by deterministic equations, 1:1 phase locking is characterized by convergence of the combined phase $\Phi(t)$ to a closed curve A (topologically a circle) called an attractor that winds around the torus in a 1:1 fashion (Fig. 2*C*). It follows that the phases $\varphi_1(t)$ and $\varphi_2(t)$ of the oscillators advance in a synchronized way and thus oscillate with a common frequency. This phase-locked state persists in the presence of weak stochasticity in the sense that typical trajectories wind around the torus in a thin band about the attractor A. However, occasionally the trajectory will go on an excursion where it leaves this band,

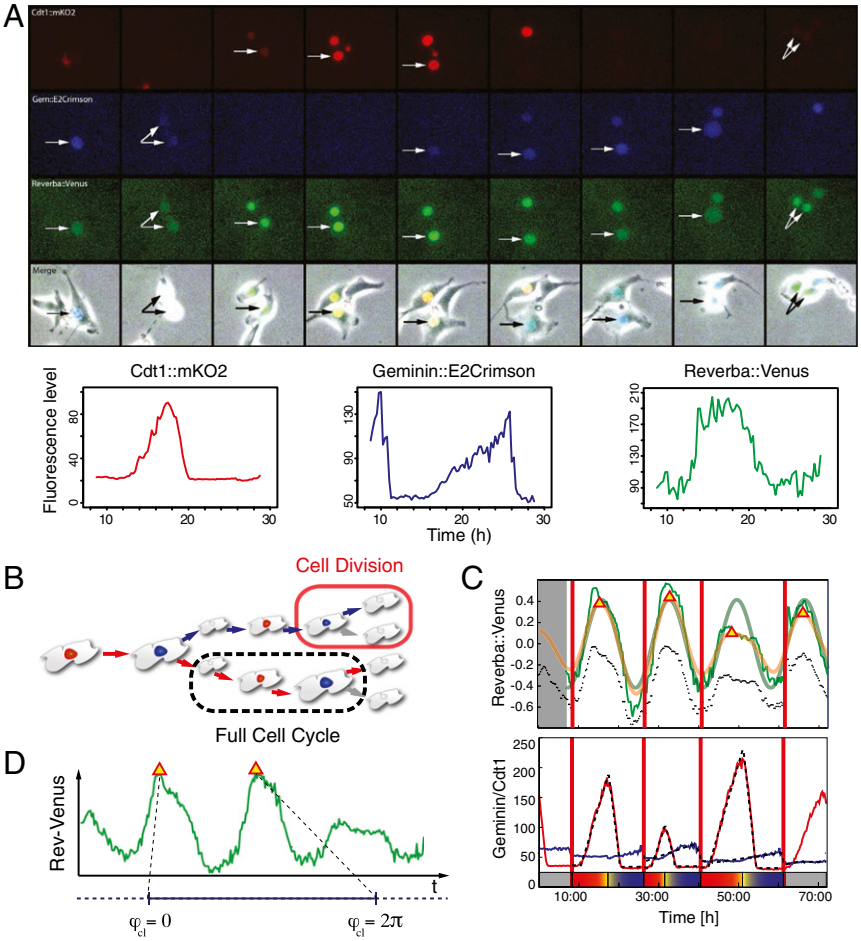

Fig. 1. Image acquisition, cell tracking, and resulting time series of NIH3T3_ Rev-Erbα::Venus_FUCCI-2A cells (see *SI Appendix* for details). (*A*) Time series of a representative single cycle for the various fluorescent reporters and respective traces in NIH3T3_ Rev-Erbα::Venus_FUCCI-2A cells (unsynchronized in 15% FBS). From top to bottom: G1 (red), Cdt1::mKO2; S/G2/M (blue), Gem::E2Crimson; Clock (green), *Rev-Erbα*::Venus; and Merge, fluorescent channels combined with the corresponding brightfield image. Arrows point to tracked cell nuclei. Images are 2.5 h apart. Traces at the bottom have been plotted from measured intensities extracted from tracking with the LineageTracker plugin for ImageJ. (*B*) Schematic of a lineage tree showing a cell division and a full cell-cycle interval. Trees are obtained using the Lineage Tracker software. (*C*) Computational analysis of the markers (72 h). (*Upper*) A detrended and a smoothed version of the *Rev-Erbα*::Venus clock marker traces (unprocessed data shown as dotted lines) appear in green and yellow, respectively. Segments at the beginning and end have been removed. We obtain an estimate for the clock period using spectrum resampling (thick green). Red triangles mark estimated clock peaks. (*Lower*) Red and blue lines represent G1 and S/G2/M cell cycle markers, respectively. We fit a piecewise linear model to both markers (shown as dashed line) and extract the time of the G1–S transition (shown on the bottom). Thick vertical lines correspond to division times as marked during tracking. (*D*) The clock phase between two clock marker peaks is defined as the relative position between the peaks, normalized to the interval $(0, 2\pi)$.

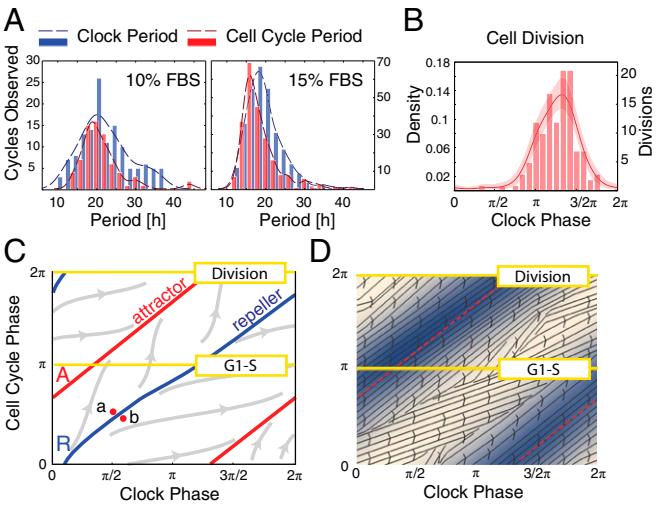

Fig. 2. Phase dynamics for unsynchronized cells. (*A*) Histograms showing distributions of periods for both the clock (blue) and cell cycle (red). Unsynchronized cells grown in 10% FBS (mean clock period, 21.9 ± 1.1 h; mean cell-cycle period, 21.3 ± 1.3 h) and 15% FBS (mean clock period, 19.4 ± 0.5 h; mean cell-cycle period, 18.6 ± 0.6 h). (*B*) Phase histograms for cells in 15% FBS; mean phase of division is 3.97 ± 0.14 radians. (*C*) Illustration of possible trajectories in 1:1 phase-locked system, showing the situation for simulated noise-free deterministic dynamics. All trajectories apart from those starting on the repeller *R* converge to the attracting periodic orbit *A*, which is a circle winding around the torus in a 1:1 fashion. Cells starting at the close points *a* and *b* will divide approximately half a clock period apart. This is what gives rise to the phase-skipping instability described in the text. Such a change in state and the consequent change in division timing can be caused by stochasticity. (*D*) Estimated phase diagram from experimental data for cells in 15% FBS (*SI Appendix*, section 2.5). The red dashed curve shows the mean trajectory and the blue levels show the density of cells passing through a region. The arrows show the mean direction that the cells flow in near that point on the torus.

joining it again approximately advanced or delayed by half a cycle. This phase-skipping phenomenon occurs when a fluctuation in the nondeterministic elements exceeds the stability domain of the attractor and initiates a phase-skipping instability as described in Fig. 2*C*.

When our data are plotted on a phase torus (Movie S2 and Fig. 2*D*), the trajectories of the unsynchronized cell lineages display all of the characteristics described above for stochastic 1:1 phase locking, and this is further confirmed by the lineage tree (Fig. 3) and the scatter plot of clock and cell cycle periods (*SI Appendix*, Fig. S3). First, the phase trajectories are relatively tightly bundled around a mean trajectory that winds around the torus in a 1:1 fashion (Fig. 2*D*). The cells in the movie generally stream along a highway given by the band about the attractor. Second, we see phase skipping as described above. Occasionally a cell moves away from the main trajectory bundle and rejoins it in a position where it has gained or lost approximately half a phase cycle. This often happens fairly soon after a division and just one of the two daughters phase-skips. Third, as a consequence of the bundling, histograms of the clock phase of cell division and G1 exit show a concentrated distribution around a mean clock phase (Fig. 2*B* and *SI Appendix*, Fig. S2 *B* and *C*).

We additionally confirmed this 1:1 phase locking at the population level in an unbiased way by fluorescence-sorting the cells by cell cycle phase and then checking whether these cells have the expected clock phase by profiling the endogenous *Rev-Erbα* mRNA (*SI Appendix*, Fig. S1 *D–F*).

We can also estimate an informative vectorfield on the torus that we use below to inform the construction of a simple mathematical model. This shows at each point on the torus the typical direction and speed of the cells as they pass near to that point (Fig. 2*D*). Although this vectorfield varies in a smooth fashion in almost all of the torus, it also has interesting defect-like structures running along an approximate curve roughly having the position of the repeller marked *R* in Fig. 2*C*. Inspection of Movie S2 shows that this is the curve where many cells are about to skip and break away from the main highway. Thus, it seems to mark the boundary of the stability domain of the attractor.

Synchronizing the Circadian Clock by Dexamethasone Reveals Further Stable Oscillating States. Treatment with the glucocorticoid agonist dexamethasone is known to exert a resetting/synchronizing effect on clocks in cultured cells through induction of *Per1* (18), and we hypothesized that this might modify the coupled dynamics. Therefore, we expanded our experiments using a dexamethasone pulse to synchronize the cells in the same conditions as above except that we used both 10% and 20% FBS to compare our results with those of Nagoshi et al. (17), who used a similar dexamethasone synchronization protocol with 20% FBS.

The synchronization resulted in a significant change in the coupled dynamics. When using 20% FBS we found that the cell lineages were dominated by two groups. The timing and clock phase of cell divisions in the first group clustered in such a way that they reproduced the three-peak distribution of clock phases of cell divisions seen by Nagoshi et al. (17) and had median periods for the clock and cell cycle of 27 h and 17 h, respectively (Fig. 4*C*), roughly a 3:2 period ratio. The cells in the second group locked 1:1 (Fig. 4*C*).

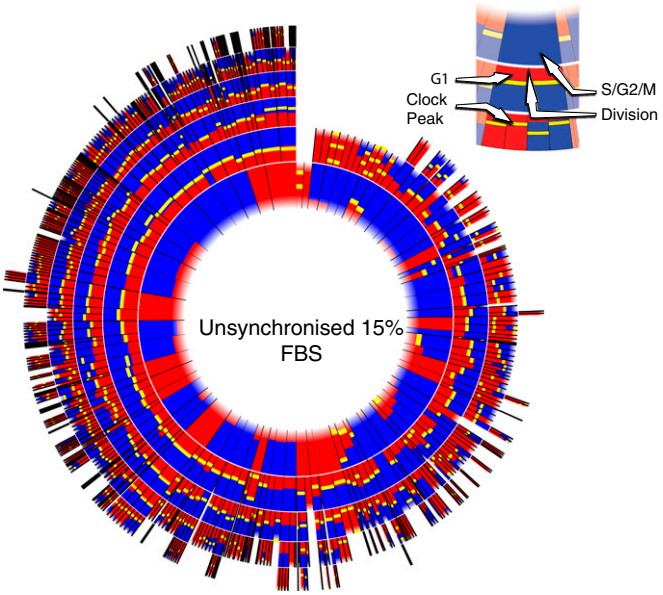

Fig. 3. Circular representations of lineage tree for unsynchronized cells in 15% FBS. Each radial segment corresponds to a cell-cycle interval we observed. Each ring corresponds to a generation of cells, starting with the first observed generation as the innermost ring. When a cell divides, its segment is split in two in the next ring outward. Because we cannot know when the first observed cell-cycle interval starts (because this time is before the start of our recording), the inner boundary is blurred. The G1 phase is drawn in red, and the S/G2/M phases are shown in blue. Clock peaks are shown as yellow bars. Times have been normalized so that all cell cycles have the same length in the plot. Thus, there is no direct correspondence between the length of a cell-cycle interval and its representation in this plot. We observe that in the unsynchronized condition the clock peaks mostly coincide with the G1–S transition.

Dexamethasone-synchronized cells in 10% FBS provide an interesting contrast. Although the synchronization significantly increased the clock period to a mean of 24.2 ± 0.5 h (from 21.9 ± 1.1 h for the unsynchronized cells), the mean cell-cycle period remained low at 20.1 ± 0.94 h, about an hour less than that observed for unsynchronized cells in 10% FBS (*SI Appendix*, Fig. S2 *A* and *B*). The population density plot of peak times of the clock marker *Rev-Erbα*::Venus and cell divisions show clear cyclicity but, strikingly, with these significantly different periods (*SI Appendix*, Fig. S2 *A* and *D*). This behavior is clearly distinct from the 1:1 phase locking seen in the unsynchronized cells in 10% FBS (*SI Appendix*, Fig. S2).

To analyze these results we found it revealing to use two different clustering algorithms to identify clusters in the timing of cell division (details in *SI Appendix*). We then plotted the clock phase of each cell division against its time as in Fig. 4 *A* and *B* and *SI Appendix*, Figs. S3–S5, highlighting the clusters identified. In both clustering approaches plotting the data in this way reveals that there is clear clustering of the cell divisions, thereby demonstrating the effect of synchronization and coupling. For the dexamethasone-synchronized cells in 20% FBS the clusters fall into two groups corresponding to the two cases identified above. The distinct identities of the two groups is further validated by the way the period ratios segregate (Fig. 4*C* and *SI Appendix*, Fig. S4*B*). Strikingly similar results were found when the dexamethasone-synchronized 20% FBS experiment was repeated (*SI Appendix*, Fig. S5*A*).

Using a simple mathematical model (Fig. 5 *A* and *B* and *SI Appendix*, Fig. S6*A* and *Methods*) we are able to analyze these dynamical regimes and integrate our findings. In this model the clock phase progresses at a constant speed and the cell cycle progresses at a speed that depends upon the phase of the clock in that it is slowed down if the joint phase of the clock and cell cycle is in the region of the torus shaded in Fig. 5 *A* and *B* (see *SI Appendix* for equations). The position of this coupling region was largely determined by using the vectorfields (Fig. 4*E* and *SI Appendix*, Fig. S7) to obtain an approximate position for the attracting periodic solution *A*, and the Poincaré maps (*SI Appendix*, Fig. S6*C*) to confirm the phases of cell division and G1-exit on *A*. Using a ratio of periods similar to the experimental ones, this model then qualitatively reproduces the observed clustering (Figs. 4 *A* and *B* and 6 and *SI Appendix*, Figs. S4 *A* and *B*, S5*A*, and S6).

We compare model results for ratios close to 3:2 and 5:4 to compare with the 20% FBS and 10% FBS dexamethasone-pulsed cases, respectively. In both cases the model produces clear clusters in the 2D plot but the projections onto the axes differ. The clustering for the 3:2 ratio gives a three-peaked distribution when projected horizontally onto the clock phase (Fig. 6*A*) but for the 5:4 ratio it gives no clear peaks because the clusters no longer line up as well in the horizontal direction (*SI Appendix*, Fig. S6*B*). This agrees with the experiments but note that in the 20% FBS dexamethasone-pulsed experiments only one of the two groups in Fig. 6*B* is populated so only half the clusters appear and they also give a three-peaked distribution. Projecting onto the time axis gives the population density plot for cell divisions. Whereas for 5:4 clear peaks are found (*SI Appendix*, Fig. S6*B*), this is not the case for 3:2 (Figs. 6*C*), a result of the different ways the peaks line up for different ratios. This agrees with our experiments (Fig. 4 and *SI Appendix*, Fig. S2) and is also consistent with the report in Nagoshi et al. (17) that cell cycle progression in their experiment was not synchronized. The fact that we reproduce the complex and apparently conflicting data coming from these different dexamethasone-pulsed experiments significantly strengths the value of this analysis.

For mathematical models of coupled oscillators, *p*:*q* phase locking is a generalization of the 1:1 locking discussed above but in this case one oscillator completes exactly *p* cycles whereas the other completes *q*. This is shown for *p*:*q* = 3:2 in Fig. 5*B*. According to the mathematical theory (6) such locking is robust but the extent of the robustness depends on the strength of the coupling and the size of *p* and *q* (when *p*:*q* is expressed in lowest-order terms) and decreases very rapidly as *p* and *q* become larger. Although *p*:*q* phase locking with $p,q > 1$ is readily seen in some low-noise physical systems we cannot expect to see it in its pure form in our stochastic system. For example, the single-cell dynamics are highly stochastic; the system kinetic parameters for daughter cells will usually vary from that of the mother and, unlike physical oscillators, the oscillator's identity is changing at division. In addition, there will be phase skipping as described above for the 1:1 case and because the stability domain of the attractor is much smaller when *p* or *q* are greater than 1, skipping will be much more common. Similarly, for such *p* and *q*, locking is sensitive to parameter variation.

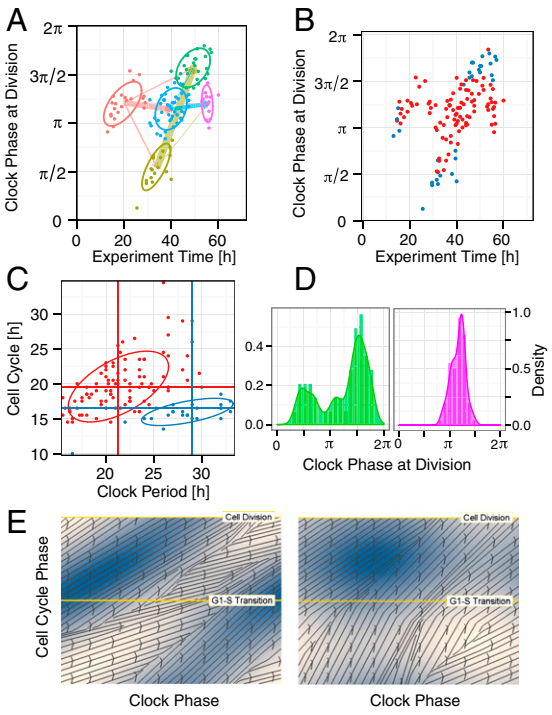

Fig. 4. Phase dynamics for cells in 20% FBS synchronized with dexamethasone. (*A* and *B*) Clustering of the scatter plot of clock phase of cell division vs. time of division using clustering method 1 (*A*) and clustering method 2 (*B*) as described in *SI Appendix*, section 2.4. These clearly identify two subpopulations of cells as described in the text. (*C*) Scatter plot of clock period vs. cell-cycle period. Each point is colored according to which of the two cluster groups it belongs to in Fig. 4*B*. We see that the cluster groups nicely segregate the two groups in terms of their period ratios. The mean periods for each of the groups are shown by the vertical and horizontal lines (blue group: clock, median 29 h, SEM 1.05 h; cell cycle, median 16.5 h, SEM 0.48 h; red group: clock, median 21.25 h, SEM 0.36 h; cell cycle, median 19.5 h, SEM 0.42 h). Each data point corresponds to a single fully observed cell-cycle interval. The *y* coordinate is the cell-cycle period and the *x* coordinate is the average length of all clock peak-to-peak intervals that overlap in time with the cell-cycle interval. There can be up to three such intervals, one from before, and two intervals for the children if there is a division. The two ellipses show the 75% confidence interval for a multivariate *t* distribution that has been fitted to the corresponding dataset. The mean period ratios for the two groups in this experiment are 1.09 and 1.80 (*SI Appendix*, Fig. S4*B* and Table S5). (*D*) Cell division densities plotted against clock phase for the two cluster groups. Note that we track lineages, and this explains the different heights of the three peaks in the *Left* plot because the middle, left, and right peaks correspond to first, second, and third divisions, respectively. (*E*) Estimated phase diagrams from experimental data for cells in 20% FBS. The left plot is for cells with an approximate 1:1 ratio and the right plot for 3:2. Details as in Fig. 2*D*.

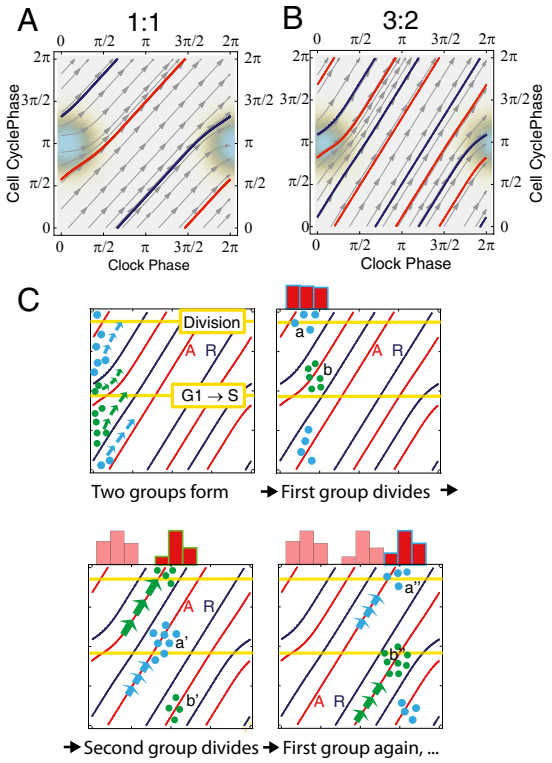

Fig. 5. Modeling of the phase-locking states in synchronized cells. (*A* and *B*) Phase portraits when winding ratios are 1:1 and 3:2. The only coupling between the clock and cell cycle occurs in the shaded region where the cell cycle is slowed down. Thus, outside this region the trajectories are straight lines. The red curve on the phase torus is the attracting periodic orbit *A* and the blue curve is the repelling periodic orbit *R* that also has to be present when the system is phase-locked. Similar results would be obtained if the cell cycle were speeded up in a similar region. (*A*) Attracting and repelling orbit for 1:1 coupling ($\nu_1 = 1, \nu_2 = 1.01$). For the deterministic, noise-free system, all trajectories that start off the repelling periodic orbit are attracted by *A*. (*B*) Attracting (red) and repelling (blue) orbit with a 3:2 winding number ($\nu_1 = 1, \nu_2 = 1.53$). (*C*) Formation of cell clusters through dexamethasone treatment. The small filled circles represent cells. After the dexamethasone pulse, the cells have roughly the same clock phase as shown by the column of cells at the left-hand side of the upper left square. Shortly afterward, they will separate into one or both of the two clusters marked a and b (*Upper Right*) because they will be attracted by orbit *A*. These clusters will then flow along *A* moving to a′ and b′ (*Lower Left*) and then at a later stage a′′ and b′′ (*Lower Right*). As they pass through the cell division phase (labeled horizontal line) we observe a burst of cell divisions resulting in the histogram shown on top of the torus.

As a result of these factors there will be a relatively broad distribution of ratios and one cannot hope to observe *p*:*q* locking in its pure form when $p,q > 1$. Nevertheless, the locking phenomenon will lead to a relevant observable experimental signature that we can hope to see when p and q are relatively small (such as 3:2), namely, a long-lived polyrhythmic behavior where the cells maintain a fluctuating fractional ratio of periods and display clustering as observed in the synchronized experiments and described below. The states observed in the dexamethasone-synchronized experiments that are not 1:1 phase-locked fit this description.

The clustering is explained in Fig. 5*C* for this 3:2 case and is due to the fact that after synchronization the cells split into either one or two groups depending on which of these branches of the attractor highway they are attracted to. These groups stay coherent because of the attraction to the attractor highway and because spreading of the clusters along the trajectory owing to the diffusive effect of stochasticity will be on a slower timescale.

Discussion

Our experiments have demonstrated that there are multiple coexisting robust oscillatory dynamical states of the coupled clock and cell cycle in proliferating mammalian cells and we have shown that varying the FBS level changes these states in a manner that accords with theory. In principle these states coexist in the same single cells because after the dexamethasone-synchronized cells are returned to dexamethasone-free regular medium there is in principle no difference between their current cellular context and that of the unsynchronized cells. This suggests that the coupled system is a stochastic dynamical system with multiple coexisting stable oscillating states and that the dexamethasone synchronization acts as a large perturbation that knocks the state out of the low-period 1:1 locked state into the domain of attraction of these other states. This is analogous to the bistability or multistability of equilibrium states that underlies many biological systems that switch between two or more different states. In our case the attractors are oscillating states and, although this is a well-known phenomenon in the theory of dynamical systems, so far as we are aware it has not been seen before in such biological systems.

The established circadian regulation of cell-cycle genes and proteins provides a consistent mechanistic basis to produce the coupling and phase locking described in our study. However, our results, together with previous observations by Nagoshi et al. (17), suggest that the coupling also operates in the opposite direction. In particular, in the unsynchronized cells, increasing FBS caused the period of both clock and cell cycle to decrease in unison with common periods that are significantly smaller than those for the clock in dexamethasone-synchronized experiments and also when the cells are confluent and not dividing. Although this is not currently supported by known mechanistic links,

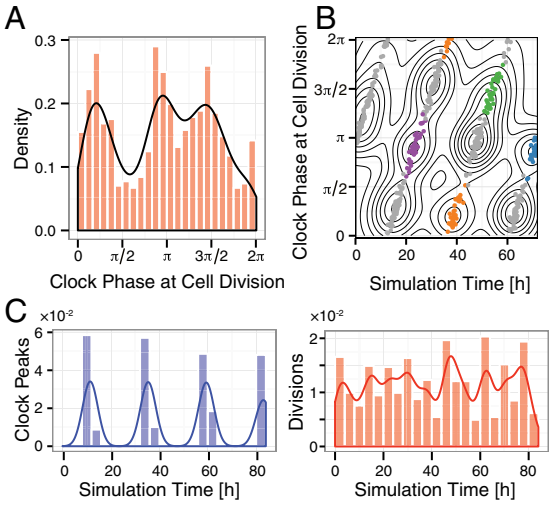

Fig. 6. Modeling stochastic 3:2 coupling. (*A*) A plot similar to Fig. 4*D*, *Left* but for modeled stochastic 3:2 coupling. In this case, we observe three peaks of cell division phases, corresponding to the three crossings of the attracting trajectory with the curve corresponding to cell division (the labeled horizontal line in Fig. 5*C*). (*B*) Clustering of the modeled cell divisions as in Fig. 4 *A* and *B*. There are essentially two sets of clusters, each group coming from (i.e., containing descendant cells of) the initial two clusters at the left. In the experiments only one of these sets is populated, presumably because of the way the synchronization works and the existence of other states (e.g., 1:1) after perturbation. This set is colored and the other is in gray. (*C*) We also see that although population-level synchronization of the clock is clear (*Left*), synchronization of cell cycle is not visible (*Right*), because the cell divisions cluster too closely in time and the projection onto the time axis is without clear peaks. We can still see the clusters of divisions in *B* when separating them out both in clock phase and time.

following ref. 17, we hypothesize that key cell-cycle events including cyclin-dependent kinase network activation, cell growth, DNA replication, nuclear envelope breakdown, cytokinesis, and reduced transcription at mitosis may rhythmically and coordinately perturb the concentration, activity, and subcellular distribution of some clock proteins and as a result modulate the period of the clock. Presumably, in vivo and in physiological situations these intracellular signals are likely to be counteracted by extracellular circadian cues such as glucocorticoids and temperature so that the clock can impose a 24-h periodicity to the cell cycle in proliferating tissues.

This and our other results suggests a natural hypothesis, namely, that (*i*) in unsynchronized cells there is bidirectional coupling enabling the clock and cell cycle to robustly entrain each other but dominated by the cell cycle, and (*ii*) dexamethasone synchronization perturbs the system into a state where the effect of the cell cycle on the clock is reduced so that the clock is freed to take up a period close to 24 h but to still regulate the cell cycle with its significantly lower natural (uncoupled) period and consequently produce both 1:1 phase-locked states and long-lived stochastic polyrhythmic states of the two coupled oscillators as observed.

Our dexamethasone-synchronized results give an interesting perspective on the question of gating as defined in the introduction. The experimental observation of clusters of cell division around multiple clock phases that we see in our dexamethasone-synchronized cells might well suggest the hypothesis that this was due to multiple gates. Indeed, Nagoshi et al. (17) expressed confidence that their trimodal frequency distribution reflected a gating by the circadian clock and noted that this gating differed from that in regenerating liver, which seemed to have a single gate. Our simple model shows that a single simple region on the torus where the clock and cell cycle couple can produce this apparent multiple gating phenomenon when no such gates exist, and, with different frequency ratios, can also produce what seems to be a single gate. Significant evidence for this phase-locking explanation over the gating hypothesis is provided by the fact that the apparent three gates seen in the 20% FBS dexamethasone-synchronized experiment (Fig. 4*D*) disappear when we change to 10% FBS (*SI Appendix*, Fig. S4*A*) and thus change the ratio of periods, but the experimental dynamics remain consistent with what we predict from the simple coupling model. The gating hypothesis is also not consistent with the dynamics seen in our unsynchronized cells. It would imply that when we plot the dynamics in the clock and cell cycle phases we should see cells waiting to go through a gate, and this is not observed (Movies S2 and S3).

It is interesting to speculate that the coexistence of multiple oscillatory states is a reflection of the need for some cellular processes to be flexible to adapt to different environmental conditions or to vary their behavior in a tissue-specific way. A loose/flexible coupling with the robust circadian clock mechanism may provide an effective and ubiquitous mechanism requiring no or minimal cell-specific rewiring of the physiologically synchronized circadian clock network.

The demonstration of robust phase locking between the mammalian clock and the cell cycle is of primary relevance to cancer because disordered circadian function has been implicated in the pathogenesis of cancer, and a deregulated cell cycle is a hallmark of cancer cells (19, 20). Of the many processes being regulated by the circadian clock, some of the most profound are those related to specific cell-cycle events, DNA repair, and apoptosis (2, 4, 5, 21–25). The dynamics of the coupling we describe here are likely to be controlled through multiple and interacting pathways. Alterations in one or several of these links may therefore compromise the robustness and the adaptability of the cell cycle–circadian clock coupled oscillator system with a broad relevance for health.

ACKNOWLEDGMENTS. We are grateful to the members of the C5Sys project for many useful discussions, particularly Albert Goldbeter and Claude Gérard. We thank S. Guérin, A. Hernandez, A. Loubat, and M. Ogier for expert technical assistance and O. Albagli for advice with the 2A system. We thank Ueli Schibler for the gift of the Rev-Erbα::Venus cell line and Eric Siggia for a critical review. This research was funded by the ERASysBio+ project C5Sys through Biotechnology and Biological Sciences Research Council (BBSRC) Grant BB/I004521/1, ZonMW Grant 90.201.127, and Agence Nationale de la Recherche (ANR) Grant ANR-2009-SYSB-002-02. Partial support was also provided by Engineering and Physical Sciences Research Council Grant GR/S29256/01 (to D.A.R.), BBSRC Grants BB/F005814/1 and BB/K003097/1 (to T.B. and D.A.R.), Netherlands Genomic Initiative/Netherlands Organization for Scientific Research Grant 050-060-510 (to G.T.J.v.d.H.), and ANR Grant ANR-11-LABEX-0028-01 (to F.D.).

1. Lowrey PL, Takahashi JS (2011) Genetics of circadian rhythms in Mammalian model organisms. *Adv Genet* 74:175–230.
2. Gréchez-Cassiau A, Rayet B, Guillaumond F, Teboul M, Delaunay F (2008) The circadian clock component BMAL1 is a critical regulator of p21WAF1/CIP1 expression and hepatocyte proliferation. *J Biol Chem* 283(8):4535–4542.
3. Kowalska E, et al. (2013) NONO couples the circadian clock to the cell cycle. *Proc Natl Acad Sci USA* 110(5):1592–1599.
4. Matsuo T, et al. (2003) Control mechanism of the circadian clock for timing of cell division in vivo. *Science* 302(5643):255–259.
5. Gery S, et al. (2006) The circadian gene per1 plays an important role in cell growth and DNA damage control in human cancer cells. *Mol Cell* 22(3):375–382.
6. Guckenheimer J, Holmes P (1983) *Nonlinear Oscillations, Dynamical Systems and Bifurcations of Vector Fields* (Springer, New York).
7. Yang Q, Pando BF, Dong G, Golden SS, van Oudenaarden A (2010) Circadian gating of the cell cycle revealed in single cyanobacterial cells. *Science* 327(5972):1522–1526.
8. Zámborszky J, Hong CI, Csikász Nagy A (2007) Computational analysis of mammalian cell division gated by a circadian clock: Quantized cell cycles and cell size control. *J Biol Rhythms* 22(6):542–553.
9. Charvin G, Cross FR, Siggia ED (2009) Forced periodic expression of G1 cyclins phase-locks the budding yeast cell cycle. *Proc Natl Acad Sci USA* 106(16):6632–6637.
10. Gérard C, Goldbeter A (2012) Entrainment of the mammalian cell cycle by the circadian clock: Modeling two coupled cellular rhythms. *PLOS Comput Biol* 8(5):e1002516.
11. Altinok A, Gonze D, Lévi F, Goldbeter A (2011) An automaton model for the cell cycle. *Interface Focus* 1(1):36–47.
12. Liu AC, et al. (2007) Intercellular coupling confers robustness against mutations in the SCN circadian clock network. *Cell* 129(3):605–616.
13. Yoo S-H, et al. (2004) PERIOD2:LUCIFERASE real-time reporting of circadian dynamics reveals persistent circadian oscillations in mouse peripheral tissues. *Proc Natl Acad Sci USA* 101(15):5339–5346.
14. Mori T, Binder B, Johnson CH (1996) Circadian gating of cell division in cyanobacteria growing with average doubling times of less than 24 hours. *Proc Natl Acad Sci USA* 93(19):10183–10188.
15. Pendergast JS, Yeom M, Reyes BA, Ohmiya Y, Yamazaki S (2010) Disconnected circadian and cell cycles in a tumor-driven cell line. *Commun Integr Biol* 3(6):536–539.
16. Yeom M, Pendergast JS, Ohmiya Y, Yamazaki S (2010) Circadian-independent cell mitosis in immortalized fibroblasts. *Proc Natl Acad Sci USA* 107(21):9665–9670.
17. Nagoshi E, et al. (2004) Circadian gene expression in individual fibroblasts: cell-autonomous and self-sustained oscillators pass time to daughter cells. *Cell* 119(5):693–705.
18. Balsalobre A, Marcacci L, Schibler U (2000) Multiple signaling pathways elicit circadian gene expression in cultured Rat-1 fibroblasts. *Curr Biol* 10(20):1291–1294.
19. Hanahan D, Weinberg RA (2011) Hallmarks of cancer: The next generation. *Cell* 144(5):646–674.
20. Levi F, Schibler U (2007) Circadian rhythms: Mechanisms and therapeutic implications. *Annu Rev Pharmacol Toxicol* 47:593–628.
21. Fu L, Pelicano H, Liu J, Huang P, Lee CC (2002) The circadian *GenePeriod2* plays an important role in tumor suppression and DNA damage response in vivo. *Cell* 111(1):41–50.
22. Oklejewicz M, et al. (2008) Phase resetting of the mammalian circadian clock by DNA damage. *Curr Biol* 18(4):286–291.
23. Granda TG, et al. (2005) Circadian regulation of cell cycle and apoptosis proteins in mouse bone marrow and tumor. *FASEB J* 19(2):304–306.
24. Kang T-H, Reardon JT, Kemp M, Sancar A (2009) Circadian oscillation of nucleotide excision repair in mammalian brain. *Proc Natl Acad Sci USA* 106(8):2864–2867.
25. Iurisci I, et al. (2006) Improved tumor control through circadian clock induction by Seliciclib, a cyclin-dependent kinase inhibitor. *Cancer Res* 66(22):10720–10728.